International Journal of Mathematical, Engineering and Management Sciences
Vol. 9, No. 6, 1483-1509, 2024
https://doi.org/10.33889/IJMEMS.2024.9.6.079

Ram Arti Publishers

# Linear and Weakly Nonlinear Stability of Thermo-Solutal Magnetoconvective Chemically Reacting Couple Stress Fluid in Porous Medium

**S. Kapoor**
Department of Mathematics,
Regional Institute of Education (NCERT), Bhubaneswar, Odisha, India.
E-mail: saurabh09.ncert@gmail.com

**A. K. Sahoo**
Department of Mathematics,
Regional Institute of Education, Utkal University, Vani Vihar, Bhubaneswar, Odisha, India.
*Corresponding author*: aksrie@gmail.com

**V. Dabral**
Department of Mathematics,
H.N.B. Garhwal University, Srinagar (A Central University),
Srinagar (Garhwal), Uttarakhand, India.
E-mail: vandana.p96@gmail.com

(Received on March 15, 2024; Revised on April 20, 2024 & August 6, 2024; Accepted on September 11, 2024)

**Abstract**
The aim of the current study is to investigate the stability analysis in case of the linear as well as nonlinear of a thermo-solutal chemically reactive couple stress fluid under uniform magnetic field convection. Investigations have been conducted on the impact of chemical reaction and external vertical magnetic field on the commencement of double diffusive convection in couple stress fluid between infinite horizontal parallel plates. Darcy's modified law governs the flow in porous media and the Oberbeck-Boussinesq approximation is accurate. For modelling the momentum equation, the modified Darcy equation with the time derivative and inertia terms is utilized. Expressions for the Rayleigh numbers with finite amplitude, oscillatory, and stationary states are found in accordance with the regulating factors. Graphics are used to illustrate how the couple-stress parameter, solute Rayleigh number, Vadasz number and diffusivity ratio affect stationary, oscillatory and finite-amplitude convection. Stationary, oscillatory and finite-amplitude convection are found to be stabilized by the couple-stress parameter and the solute Rayleigh number. The normal mode analysis method is utilized to look into the linear stability of flow dynamics after the nonlinear mathematical problem has been linearized. When stationary and finite-amplitude modes are present, the diffusivity ratio has a destabilizing effect; when oscillatory convection is present, it has a dual effect. Oscillatory convection develops earlier when the Vadasz number is higher. The couple-stress parameter and diffusivity ratio both increase with increasing solute Rayleigh number values, but the heat and mass transfer decreases as these values rise. Using double Fourier series, a generalized weakly nonlinear stability analysis is done. The research illustrates how various regulating parameters support and destabilize the flow dynamics. The influence of finite-amplitude convection on stability is also examined. Furthermore, the best conditions for stationary and oscillatory convection are based on altering the couple stress flow stability by controlling the applied magnetic field.

**Keywords**- Magnetoconvection, Thermo-solutal, Chemical reaction, Linear and nonlinear Stability, Couple stress fluid, Porous medium.

## List of Symbols

***Latin Symbols***

| | |
|---|---|
| Acceleration due to gravity, $(0, 0, -g)$ | : $g$ |
| Amplitude of concentration perturbation | : $E_{mn}$ |
| Amplitude of streamline perturbation | : $A_{mn}$ |
| Amplitude of thermal perturbation | : $B_{mn}$ |

Couple-stress parameter, where $C$ is equal to $\frac{\mu_C}{\mu D^2}$ : $C$
Equilibrium solute concentration : $S_{Eq}$
Height in case of the fluid layer : $d$
Helical force parameter : $S_h$
Hydromagnetic parameter : $H_m$
Nusselt number : $\mathrm{N_u}$
Permeability in case of porous medium : $k$
Prandtl number : $Pr$
Pressure : $p$
Sherwood number : $Sh$
Solute Rayleigh number, $\frac{\Delta S d k g \beta_S}{\nu \kappa_S}$ : $Ra_S$
Solute concentration : $S$
Space coordinates : $x, y, z$
Taylor number : $Ta$
Thermal Rayleigh number, $\frac{\Delta T d k g \beta_T}{\nu \kappa_T}$ : $Ra_T$
Temperature : $T$
Thermal conductivity : $K$
Time : $t$
Vadasz number, $\frac{\varepsilon \nu d^2}{\kappa_T k}$ : $Va$
Velocity vector, $(u, v, w)$ : $q$
Wavenumbers considered along the horizontal plane : $l, m$

***Greek Symbols***

Coefficient of solute expansion : $\beta_S$
Coefficient of thermal expansion : $\beta_T$
Couple-stress viscosity : $\mu_C$
Density : $\rho$
Diffusivity ratio, $\frac{K_S}{K_T}$ : $\tau$
Dimensionless concentration : $\varphi$
Dimensionless temperature : $\theta$
Dynamic viscosity : $\mu$
Epsilon : $\varepsilon$
Frequency : $\omega$
Growth rate : $\sigma$
Kinematic viscosity, $\nu = \frac{\mu}{P_0}$ : $\nu$
Solute diffusivity : $K_S$
Stream function : $\psi$
Thermal diffusivity : $K_T$
Wavenumber : $\alpha$

***Subscript***

Basic state : $b$
Critical state : $c$
Reference value : $0$

***Superscript***

| | |
|---|---|
| Dimensionless quantity | : $*$ |
| Oscillatory | : $osc$ |
| Perturbed quantity | : $'$ |
| Stationary | : $st$ |

## 1. Introduction

Since there are so many applications for linear stability of heat transfer across a porous media, it has become interesting to study the associated transport mechanisms. Porous media is reported by Nield and Bejan and the theory of convection in porous media is well documented in the book of Nield and Bejan (2006). Shubov and Edwards (2006) focused on analysing the stability of a fluid flow moving through a channel where the walls are flexible, meaning they can deform in response to the fluid pressure, investing the conditions under which the flow remains stable or becomes unstable due to these wall interactions. The primary goal is to analyse the stability of the fluid flow by examining the behaviour of small perturbations to the steady solution. This involves determining the conditions under which these perturbations grow exponentially for unstable flow or decay for stable flow. This research has relevance to understanding blood flow dynamics in arteries, where the arterial walls can be considered flexible and can influence the stability of blood flow. This interest is sparked by the wide range of situations that can be approximated or described as transport via porous surfaces, including packed spherical beds, very effective building insulation, chemical catalytic reactors, grain storage, and many more. Wind turbines, rocket engines, oil pipelines and air conditioning systems are some industrial applications.

Research on mass convective flow and heat transfer through chemical reactions with heat sources can be useful in many engineering and scientific domains. Temperature differences, concentration differences, as well as a combination of factors, all contribute to the frequent occurrence of natural convection flows in nature. Controlling the heat and mass transmission requires an understanding of the heat source and the outcomes of chemical reactions.

Recently, researchers have looked into the equally significant issue of hydromagnetic convective flow of a conducting fluid through a porous media. It is crucial to understand magnetohydrodynamic (MHD) effects in a variety of contexts, including plasma engineering, MEMS technology, and thin-film materials technology. Attention has gradually shifted to this field as a result of numerous applications in Chang and Chen (1998), Jang and Lee (2000), Herdrich et al. (2006) and Chen and Lai (2010). In reality, stabilizing the flow of a film by using a magnetic field has two benefits: (1) no mechanical or electrical contact with the fluid is required; and (2) straight forward active control of a technological process.

Researchers like Patil and Rudraiah (1973), Rudraiah and Vortmeyer (1978), Rudraiah (1984), Alchaar et al. (1995a, b) and Bian et al. (1996a, b) have studied the issue of magneto-convection in a porous media. Gaikwad et al. (2009a, b) performed an analytical analysis of linear and nonlinear double-diffusive convection in a fluid-saturated anisotropic porous layer with Soret and cross-diffusion effects. Zaho et al. (2014) used linear and weakly nonlinear stability analysis to study the double-diffusive convection in a Maxwell fluid-saturated porous layer with an internal heat source. Thermosolutal convection in a couple-stress fluid, including the effects of helical force and rotation, was studied by Nagaraju et al. (2023) in terms of linear and weakly nonlinear stability studies. By utilizing the standard modes, the controlling nondimensional equations can be resolved. In this case, thermosolutal convection in a couple-stress fluid has been subjected to linear and weakly nonlinear stability assessments. The normal modes are also used to solve the governing nondimensional equations.

Srivastava et al. (2012) have studied thermal instability in an electrically conducting two-component Boussinesq fluid-saturated-porous medium with the Soret effect and a constant vertical magnetic field. The impact of local thermal non-equilibrium (LTNE) on the start and heat transport phenomena of steady Brinkman-Bénard convection was investigated by Siddheshwar and Siddabasappa (2017).

In this manuscript, a linear and weakly nonlinear stability is done. Some significant discoveries on the beginning of convection in a highly permeable vertical porous layer with open boundaries have been emphasized by Barletta and Rees (2019). Kaloni and Lou (2002) have studied the stability of thermally driven shear flow of an Oldroyd-B fluid heated from below. Malashetty and Kollur (2011) studied analytically the double-diffusive convection in horizontal couple stress fluid-saturated anisotropic porous layer, which is heated and salted from below. A study by Kumar et al. (2020) used linear instability and nonlinear energy analysis to probe the double-diffusive instability in an inclined porous layer with a concentration-based internal heat source. In this case, they have implemented a porous layer and the idea of double-diffusive convection.

The stability of penetrative convection in a couple-stress fluid with internal heat source effect was examined by Mahajan and Nandal (2017) and Nandal and Mahajan (2018). In networks of chemical reactions, Muyinda et al. (2018) have investigated the linear stability of the FDM scheme. In this study, asymptotic and linear stability are discussed in depth with reference to Kim and Cardoso (2018) investigation of the impact of diffusivity ratio on the start of the buoyancy-driven instability of an A + B C chemical reaction system in a Hele-Shaw cell. The global stability of the couple stress fluid was reported by Choudary (2019). Umavathi and Bég (2020) investigated how to model the onset of thermosolutal convective instability in a layer of porous non-Newtonian nanofluid. In the absence of gravity, Mendis et al. (2020) investigated the global linear stability of convection in case of thermo-solutal Marangoni in a liquid bridge.

A study on the linear and nonlinear stability analysis of double diffusive electro-convection in couple stress anisotropic fluid-saturated rotating porous layer has been conducted by Mishra et al. (2022). Choudhary et al. (2023) study the tangent hyperbolic fluid MHD thermal and solutal stratified stagnation flow caused by extending cylinder with dual convection. Harfash and Meften (2018) studied the problem of convective movement of a reacting solute in a viscous incompressible fluid occupying a plane layer and subjected to a couple stresses effect, which is used in the present context. A Darcy-Brinkman porous layer that was heated and salted below was used to study the double-diffusive convection with chemical reaction by Mahajan and Tripathi (2021). The energy method is used to undertake nonlinear analysis, whereas performing linear analysis, the normal mode approach is employed. When compared to the solutal contribution of the chemical reaction, it is discovered that the thermal contribution of the reaction has a greater effect on convective instability. All the techniques in Mahajan and Tripathi (2021) along with other methods are used in the current study.

Mishra et al. (2022) investigated the influence of rotation and electric field on the onset of double-diffusive convection in rotating anisotropic couple stress fluid embedded porous media, which is caused by the combined action of external AC electric field and heating from below. Using the modified Brinkman model and the normal mode approach, the corresponding equations were solved. In the present study the horizontal layer has been heated from below and normal mode technique has also been employed. Shivakumara et al. (2016) conducted linear and weakly nonlinear stability assessments on two-dimensional magnetoconvection in a Brinkman porous media layer using the local thermal nonequilibrium (LTNE) model. Linear stability analysis yields the conditions for the presence of both stationary and oscillatory convection. We provide results of stationary and oscillatory convection as well as studies of linear and weakly nonlinear stability.

The onset of convection in a porous medium saturated by a heated and salted Oldroyd-type viscoelastic fluid is examined by Bharty et al. (2023) by taking into account the effects of chemical reactions on boundaries and externally imposed magnetic fields with non-equilibrium temperature conditions. In this instance, the linear stability analysis process is conducted using the normal mode approach. We have included the chemical reaction parameter and linear stability analysis in the current study.

Rana and Khurana (2023) analysed the stability of a non-Newtonian nanofluid layer subjected to chemical reaction, rotation and magneto-convection. Linear and non-linear stability assessments are carried out using Buongiorno's two-phase model with two dominating slip mechanisms, which is based on partial differential equations. Here the corresponding linear and non-linear stability techniques have been implemented in the present study.

The onset of convection in a porous medium saturated by a viscoelastic fluid of the Oldroyd type, heated and salted from below, was studied by Bharty et al. (2024) by taking into account the effects of chemical reactions on boundaries and externally imposed magnetic fields with non-equilibrium temperature conditions. The linear stability analysis in this instance is based on the normal mode approach. Additionally, the Chandrasekhar number is introduced and linear stability analysis is used in this study.

Keeping in view of the above contributions, it is observed that none of the authors has attempted to work in the direction of current work. In the present paper an investigation of linear and nonlinear stability of magneto-convection in a porous medium has been attempted. The associated equations have been solved using the normal mode technique. Finally, neutral stability curves illustrating the influence of different flow parameters on neutral stability have been sketched. Furthermore, the mass and heat transmission have been studied using a weak non-linear stability analysis.

## 2. Mathematical Formulations of the Problem

We have taken into account a horizontal porous layer heated and salted from below and considered between two parallel infinite stress-free barriers, $z = 0, d$, saturated with a couple-stress fluid in **Figure 1**.

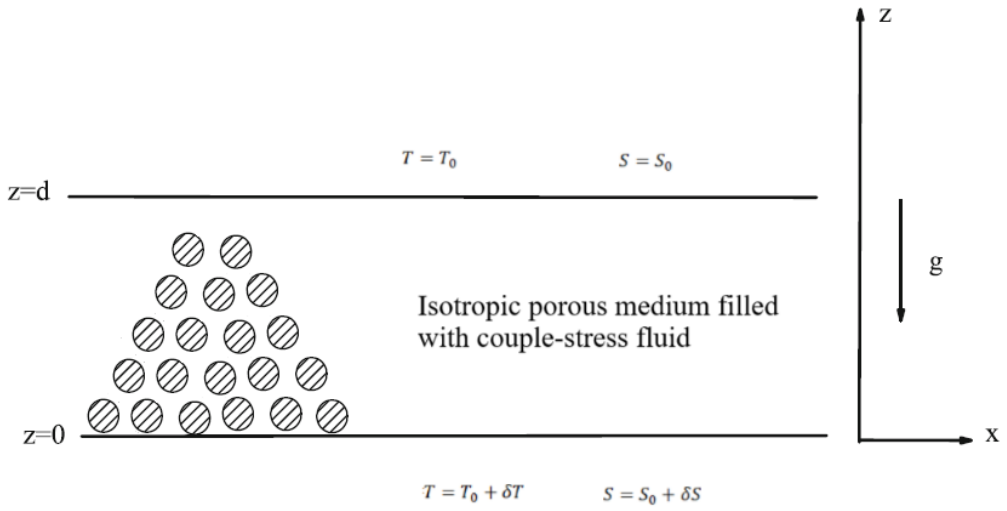


**Figure 1.** Physical configuration.

The cartesian coordinate system (with the $z-$axis oriented vertically upward) depicts the gravitational field; the bounding plane variations in temperature and concentration are $T$ and $S$, respectively. The physical configuration is depicted in **Figure 1**. In addition to the modified Darcy's law, which depicts the flow in the porous media, we believe that the Oberbeck-Boussinesq approximation is valid. The following basic formulae can be used to study the convection in the case of a double-diffusive and in a horizontal porous layer saturated with couple-stress fluid:

$$\nabla . q = 0 \tag{1}$$

$$\nabla . H_m = 0 \tag{2}$$

$$\frac{\rho_0}{\varepsilon}\left(\frac{\partial \mathrm{q}}{\partial \mathrm{t}} + \frac{1}{\varepsilon} q . \nabla q\right) = -\nabla p + \rho g - \frac{1}{k}(\mu - \mu_c \nabla^2) q + \mu_m H_m \nabla H_m \tag{3}$$

$$\frac{\partial H_m}{\partial t} + q . \nabla H_m - H_m . \nabla q = \eta \nabla^2 H_m \tag{4}$$

$$\gamma \frac{\partial \mathrm{T}}{\partial \mathrm{t}} + (\mathrm{q} . \nabla)\mathrm{T} = \kappa_T \nabla^2 T + Q_0 \nabla T \tag{5}$$

$$\varepsilon \frac{\partial \mathrm{S}}{\partial \mathrm{t}} + (\mathrm{q} . \nabla)\mathrm{S} = \kappa_S \nabla^2 S + k\left(S_{Eq}(T) - S\right) \tag{6}$$

$$\rho = \rho_0[1 - \beta_T(T - T_0) + \beta_S(S - S_0)] \tag{7}$$

Because of the thermo-solutal boundary conditions

$T = T_0 + \delta T$, at $z = 0$ and $T = T_0$ at $z = d$,

$S = S_0 + \delta S$, at $z = 0$ and $S = S_0$ at $z = d$ (8)

Further,

$$\gamma = \frac{(\rho c)_m}{(\rho c_p)_f},\ \kappa_T = \frac{(1-\varepsilon)\mathrm{K_S} + \varepsilon \mathrm{K_f}}{(\rho c_p)_f}, (\rho c)_m = (1 - \varepsilon)(\rho c)_s + \varepsilon \left(\rho c_p\right)_f .$$

Here, the fluid has the specific heat $c_p$ when pressure is constant; for the given solid $c$ is the specific heat; and the subscripts $m, s$ and $f$ denote porous, solid and fluid medium values, respectively.

## 3. Basic State

It is believed that the fluid is in a fundamental state of quiescence, as shown by

$$q_b = (0,0,0),\ p = p_b(z),\ T = T_b(z),\ S = S_b(z), \rho = \rho_b(z), H_m = (H_m)_b(z) \tag{9}$$

The following equations are satisfied by the temperature $T_b(z)$, solute concentration $S_b(z)$, pressure $p_b(z)$ and density $\rho_b(z)$:

$$\frac{dp_b}{dz} = \rho_b g \tag{10}$$

$$\frac{d^2 T_b}{dz^2} = 0 \tag{11}$$

$$\frac{d^2 S_b}{dz^2} = 0 \tag{12}$$

$$\rho_b = \rho_0[1 - \beta_T(T_b - T_0) + \beta_S(S_b - S_0)] \tag{13}$$

The solution to the problem of basic temperature and concentration is

$$T_b = T_0 + \delta T\left(1 - \frac{z}{d}\right) \text{ and } S_b = S_0 + \delta S\left(1 - \frac{z}{d}\right) \tag{14}$$

However, using Equations (13) and (14) which are no longer necessary, one can still arrive at the fundamental solution to the pressure field.

## 4. Linear Stability Analysis

In order to perform the linear stability, the adopted procedure is well documented in the book of Drazin (2012). The detailed procedure is given below:

### 4.1 Disturbance Equation

The stability of the fundamental state is investigated by using linear theory. The basic state, which has the following shape, experiences a tiny perturbation.

$$q = q_b + q'(x,y,z,t), T = T_b(z) + T'(x,y,z,t),$$

$$S = S_b(z) + S'(x,y,z,t), p = p_b(z) + p'(x,y,z,t),$$

$$\rho = \rho_b(z) + \rho'(x,y,z,t), H_m{}' = (H_m)_b + h'(x,y,z,t) \quad (15)$$

where, the primes represent the slightest probable disruption. The linear disturbance equation can be created by using Equation (15) in Equations (1) - (7).

$$\nabla . q' = 0 \quad (16a)$$

$$\nabla . h' = 0 \quad (16b)$$

$$\frac{\rho_0}{\varepsilon}\left(\frac{\partial q'}{\partial t} + \frac{1}{\varepsilon} q' . \nabla q'\right) = -\nabla p' + \rho' g - \frac{\mu}{k}\left(1 - \frac{\mu_c}{\mu}\nabla^2\right) q' + \mu_m (H_m)_b \nabla h \quad (17)$$

$$\gamma \frac{\partial T'}{\partial t} + (q' . \nabla) T' + w' \frac{\partial T_b}{\partial z} = \kappa_T \nabla^2 T' + Q_{hs} T' \quad (18)$$

$$\varepsilon \frac{\partial S'}{\partial t} + (q' . \nabla) S' + w' \frac{\partial S_b}{\partial z} = \kappa_S \nabla^2 S' + k\left(S_{Eq}(T') - S\right) \quad (19)$$

$$\rho' = -\rho_0 (\beta_T T' - \beta_S S') \quad (20)$$

### 4.2 Non-dimensional Equations

In this context, two-dimensional disturbances are taken into account, allowing us to define stream function $\psi$ and $\phi$ as follows:

$$(u', w') = \left(-\frac{\partial \psi}{\partial z}, \frac{\partial \psi}{\partial x}\right), \; h' = \left(\frac{\partial \phi}{\partial z}, -\frac{\partial \phi}{\partial x}\right) \quad (21)$$

which meet the criteria for continuity equation. By inserting the stream function $\psi$ in Equation (17), the pressure is eliminated. Equations (16a), (16b) and (17) are then nondimensionalized using the following non-dimensional parameters.

$$(x^*, z^*) = \left(\frac{x}{d}, \frac{z}{d}\right), \; t^* = t\left(\frac{\gamma d^2}{\kappa_T}\right), \psi^* = \frac{\psi}{\kappa_T}, T^* = \frac{T'}{\Delta T}, S^* = \frac{S'}{\Delta S},$$

$$h_z' = h_z^* (H_m)_b \quad (22)$$

We obtain

$$\left(\frac{1}{\gamma V_a}\frac{\partial}{\partial t} + 1 - C\nabla^2\right)\nabla^2 \psi - \frac{1}{V_a}\left(\frac{\partial \psi}{\partial x}\frac{\partial (\nabla^2 \psi)}{\partial z} - \frac{\partial \psi}{\partial z}\frac{\partial (\nabla^2 \psi)}{\partial x}\right) = -Ra_T \frac{\partial T}{\partial x} + Ra_S \frac{\partial S}{\partial x} + C_h M_p \nabla^2 \frac{\partial \phi}{\partial z} \quad (23)$$

$$\left(\frac{\partial}{\partial t} - C_h M_p \nabla^2\right)\phi = \frac{\partial \psi}{\partial z} \quad (24)$$

$$\frac{\partial T}{\partial t} + \frac{\partial \psi}{\partial x} - \left(\frac{\partial \psi}{\partial x}\frac{\partial T}{\partial z} - \frac{\partial \psi}{\partial z}\frac{\partial T}{\partial x}\right) - \nabla^2 T - QT' = 0 \quad (25)$$

$$\frac{\varepsilon}{\gamma}\frac{\partial S}{\partial t}+\frac{\partial \psi}{\partial x}-\left(\frac{\partial \psi}{\partial x}\frac{\partial S}{\partial z}-\frac{\partial \psi}{\partial z}\frac{\partial S}{\partial x}\right)-\tau\nabla^2 S=\chi(T-S) \tag{26}$$

Here, $Ra_T=\frac{\beta_T g\Delta T dk}{\nu\kappa_T}, V_a=\frac{\varepsilon\nu d^2}{\kappa_T k}, Ra_S=\frac{\beta_S g\Delta S dk}{\nu\kappa_S}, C=\frac{\mu_c}{\mu d^2}, \tau=\frac{\kappa_S}{\kappa_T}$.

The dimensionless groups that appear are thermal Rayleigh number ($Ra_T$), Vadasz number ($V_a$), solute Rayleigh number ($Ra_S$), Chandrasekhar number ($C_h$), couple-stress parameter ($C$), diffusivity ratio ($\tau$) and Magnetic Prandtl number ($M_p$).

For ease of use, the asterisks have been removed. The Equations (23) and (24) can also be combined. The new equation is going to be

$$\left(\frac{1}{\gamma V_a}\frac{\partial}{\partial t}+1-\mathrm{C}\nabla^2\right)\left(\frac{\partial}{\partial t}-C_h M_p\nabla^2\right)\nabla^2\psi-\frac{1}{V_a}\left(\frac{\partial}{\partial t}-C_h M_p\nabla^2\right)\left(\frac{\partial \psi}{\partial x}\frac{\partial(\nabla^2\psi)}{\partial z}-\frac{\partial \psi}{\partial z}\frac{\partial(\nabla^2\psi)}{\partial x}\right)=$$
$$-Ra_T\left(\frac{\partial}{\partial t}-C_h M_p\nabla^2\right)\frac{\partial T}{\partial x}+Ra_S\left(\frac{\partial}{\partial t}-C_h M_p\nabla^2\right)\frac{\partial S}{\partial x}+C_h M_p\nabla^2\frac{\partial^2\psi}{\partial z^2} \tag{27}$$

We set the values of $\varepsilon$ and $\gamma$ to unity to limit the number of parameters. Equations (22) - (26), which have the boundary conditions of being stress-free, isothermal and vanishing couple-stress are solved.

$$\psi=\frac{\partial^2\psi}{\partial z^2}=\frac{\partial^4\psi}{\partial z^4}=T=S=0, \text{ at } z=0,1 \tag{28}$$

The mathematical simplicity of the stress-free boundary conditions is chosen without sacrificing physically significant qualitative impacts. Although it is a useful mathematical simplification, the application of stress-free boundary conditions is not physically sound. The problem cannot be solved analytically if the proper boundary conditions are rigid-rigid boundary conditions.

## 5. Method of Solution

The local non-linear stability analysis discussed in the following benefits greatly from the use of the linear stability analysis. To carry out this study, we assume that the solutions to Equations (22) - (26) are periodic waves of the form by ignoring the Jacobian.

$$\begin{pmatrix}\psi\\T\\S\end{pmatrix}=e^{\sigma t}\begin{pmatrix}\psi_0\, sin\, n\pi\alpha x\\ \theta_0\, cos\, n\pi\alpha x\\ \Phi_0\, cos\, n\pi\alpha x\end{pmatrix}sin(n\pi z)\quad (n=1,2,3,\dots) \tag{29}$$

where, the growth rate, $\sigma$, is usually a complex variable ($\sigma=\sigma_r+i\sigma_i$) and $\alpha$ is the horizontal wave number. Equation (29) is substituted for Equations (22) - (26), resulting in the following.

$$\left[\left(\frac{\sigma}{\gamma V_a}+1-\mathrm{C}\right)(\sigma-C_h M_p\delta_\mathrm{n}^2)\delta_\mathrm{n}^2-C_h M_p \mathrm{n}^2\pi^2\right]\psi_0\,\delta_\mathrm{n}^2\sin(n\pi\alpha x)-n\pi\alpha(\mathrm{Ra_T}\theta_0-$$
$$\mathrm{Ra_S}\Phi_0)\left[\sigma\sin(n\pi\alpha x)+C_h M_p\delta_\mathrm{n}^2\cos(n\pi\alpha x)\right]=0 \tag{30}$$

$$n\pi\alpha\psi_0+(\sigma+\delta_\mathrm{n}^2-\mathrm{Q})\theta_0=0 \tag{31}$$

$$\sigma n\pi\alpha\psi_0-\chi\theta_0+(\sigma+\tau\delta_\mathrm{n}^2+\chi)\Phi_0=0 \tag{32}$$

where, $\delta_\mathrm{n}^2=n^2\pi^2(M_p\alpha^2+1)$, $\eta=1+C\ \delta_\mathrm{n}^2$. The couple stress viscosity of the fluid is represented by the parameter $\eta$. We have $\eta=1$ in the case of Newtonian fluid. Equations from (30) - (32) can now be expressed in matrix form as:

$$AX=0 \tag{33}$$

where,

$$A = \begin{pmatrix} \mathrm{P} & \mathrm{Ra_T} n\pi\alpha\left(\sigma + C_h M_p \delta_n^2\right) & -\mathrm{Ra_S} n\pi\alpha\left(\sigma + C_h M_p \delta_n^2\right) \\ n\pi\alpha & \sigma + \delta_n^2 - \mathrm{Q} & 0 \\ \sigma n\pi\alpha & -\chi & \sigma + \tau\delta_n^2 + \chi \end{pmatrix}.$$

$$X = \begin{pmatrix} \psi_0 \\ \theta_0 \\ \Phi_0 \end{pmatrix} \text{ and } 0 = \begin{pmatrix} 0 \\ 0 \\ 0 \end{pmatrix}.$$

$$\mathrm{P} = \left[\frac{\sigma^2}{V_a}\left(1 + C_h M_p \delta_n^2\right) + \eta\left(\sigma + C_h M_p \delta_n^2\right) + C_h M_p \mathrm{n}^2\pi^2 + (n\pi^2 1) C_h\right]\delta_n^2.$$

We need the determinant of the matrix A to disappear for a non-trivial solution for X, which results in:

$$Ra_T = \frac{AX\delta_n^2(\sigma+\delta_n^2-\mathrm{Q})(\sigma+\tau\delta_n^2+\chi)+Ra_S n^2\pi^2\alpha^2(\sigma+C_h M_p\delta_n^2)(\chi+\sigma^2+\sigma\delta_n^2-\sigma\mathrm{Q})}{n^2\pi^2\alpha^2(\sigma+C_h M_p\delta_n^2)(\sigma+\tau\delta_n^2+\chi)} \quad (34)$$

where, $A = \left[\frac{\sigma^2}{V_a}\left(1 + C_h M_p \delta_n^2\right) + \eta\left(\sigma + C_h M_p \delta_n^2\right) + C_h M_p \mathrm{n}^2\pi^2\right]$.

As usual, we limit our study to the scenario when $n = 1$ (fundamental mode) is the most unstable mode (for more information, see Chandrasekhar (1981) for details). Consequently, we put $\eta = 1 + C\delta^2$ in our further analyses and $\delta^2 = \pi^2(\alpha^2 + 1)$.

### 5.1 Stationary State

For stable state, we have σ = 0 at the marginal stability. In stable steady mode, the Rayleigh number is as follows:

$$Ra_T^{st} = \frac{(\eta\delta_n^2+\mathrm{n}^2\pi^2)(\delta_n^2-\mathrm{Q})(1+\pi^2)\mathrm{C_h}}{\mathrm{n}^2\pi^2\alpha^2} + \frac{Ra_S(\chi+\delta_n^2)}{\tau\delta_n^2+\chi} \quad (35)$$

For $n = 1$,

$$Ra_T^{st} = \frac{(\eta\delta^2+\pi^2)(\delta^2-\mathrm{Q})(1+\pi^2)\mathrm{C_h}}{\pi^2\alpha^2} + \frac{Ra_S(\chi+\delta^2)}{\tau\delta^2+\chi}.$$

Minimal value of the Rayleigh number is $Ra_T^{st}$ happens at the wavenumber $\alpha = \alpha_c$, where the following equation is satisfied by $\alpha_c$.

$$2C\pi^2(\alpha^2)^2 + (1 + C\pi^2)\alpha^2 - (1 + C\pi^2) = 0 \quad (36)$$

It is significant to remember that the couple-stress parameter $C$ affects the critical wavenumber $\alpha_c$. Equation (35) results in the single-component system when $Ra_S = 0$ as given below:

$$Ra_T^{st} = \frac{(\eta\delta^2+\pi^2)(\delta^2-\mathrm{Q})(1+\pi^2)\mathrm{C_h}}{\pi^2\alpha^2} \quad (37)$$

Equation (36) gives the critical Rayleigh number in the presence of couple stresses.

$$Ra_{T,c}^{st} = \frac{\left(\pi^2{\alpha_c}^2+\pi^2-Q\right)(\pi^2+1)\mathrm{C_h}\left[{\alpha_c}^2+2+C\pi^2\left(1+{\alpha_c}^2\right)^2\right]}{{\alpha_c}^2} \quad (38)$$

From Equation (36), the critical wave number $\alpha_c$ is to be found. These values exactly match those provided by Siddheshwar and Pranesh (2004) for a fluid system with a single component under couple stress. Additionally, when $C = 0$ and couple tensions are absent, Equation (37) gives

$$Ra_T^{st} = \frac{(\pi^2\alpha^2+\pi^2-Q)(\pi^2+1)[2+\alpha^2]C_h}{\alpha_c{}^2} \quad (39)$$

where, through a Darcy porous layer the critical values for a Newtonian fluid flowing and heated from below are $\alpha_c = 1$ and $Ra_T^{st} = 4\pi^2$.

### 5.2 Oscillatory State

Equation (34) is modified by adding the components $n = 1$ and $\sigma = i\omega$ ($\omega$ is real) to obtain the oscillatory Rayleigh number $Ra_T^{osc}$ at the stability margin.

$$Ra_T^{osc} = \frac{\left[\left\{-\frac{\omega^2}{V_a}\left(1+C_hM_p\delta^2\right)+\eta(i\omega+C_hM_p\delta^2)+C_hM_p\pi^2\right\}\delta^2(i\omega+\delta^2-Q)(i\omega+\tau\delta^2+\chi)\right]+ Ra_S\pi^2\alpha^2(i\omega+C_hM_p\delta^2)(-i\omega^2+i\omega\delta^2-i\omega Q+\chi)}{\pi^2\alpha^2(i\omega+C_hM_p\delta^2)(i\omega+\tau\delta^2+\chi)} \quad (40)$$

where,

$\omega^2$ is a non-dimensional frequency that takes the following form:

$$\omega^2 = \frac{\delta^2\left(\delta^2-\frac{\alpha^2}{V_a}\right)[\alpha^2+\delta^4(1+\chi)]-\alpha^2\delta^4\left(1+\frac{1}{V_a}\right)}{(\delta^2-Q)[\delta^4(1+\chi)^2+\alpha^2]} \quad (41)$$

To understand their influence on the onset of oscillatory convection, the oscillatory Rayleigh number given by Equation (38) is analytically reduced numerically with regard to the wave number. Only if $\tau < 1$ is present, according to a close examination of the expression for frequency $\omega$, is oscillatory convection possible. The values of the solute Rayleigh convection that takes place before stationary convection are described in detail for a range of values of the couple-stress parameter, Vadasz number, and diffusivity ratio.

## 6. A Weak Nonlinear Stability Theory

This section analyzes the weakly nonlinear stability of the stream function $\psi$, temperature $T$, and concentration $S$ using a Fourier series representation.

$$\psi = \sum_{m=1}^{\infty}\sum_{n=1}^{\infty} D_{mn}(t)\, sin(m\pi\alpha x)\sin(n\pi z) \quad (42)$$

$$T = \sum_{m=0}^{\infty}\sum_{n=1}^{\infty} E_{mn}(t)\, cos(m\pi\alpha x)\sin(n\pi z) \quad (43)$$

$$S = \sum_{m=1}^{\infty}\sum_{n=1}^{\infty} F_{mn}(t)\, cos(m\pi\alpha x)\sin(n\pi z) \quad (44)$$

$$\varphi = \sum_{m=1}^{\infty}\sum_{n=1}^{\infty} G_{mn}(t)\, cos(m\pi\alpha x)\sin(n\pi z) \quad (45)$$

We construct a system of coupled, nonlinear ordinary differential equations by substituting Equations (42) – (45) into the set of coupled nonlinear partial differential Equations (1) - (7). However, it makes sense to make use of the fact that flows in suspensions are frequently dominated by a small number of spatial harmonics in laboratory systems and real-world scenarios.

The interaction between $\psi$, T and also $\psi$, S enables the temperature and concentration fields to deviate as the initial effect in case of nonlinearity. These fields will distort, leading to a shift in the horizontal mean and the generation of a component of the form $sin\,(2\pi z)$. As a result, the following simple Fourier series can be used to represent a finite-amplitude double-diffusive convection:

$$\psi = D_1(t)\, sin(\pi\alpha x)sin(\pi z) \quad (46)$$

$$T = E_1(t)\, cos(\pi\alpha x) sin(\pi z) + E_2(t)\, sin(2\pi z) \quad (47)$$

$$S = F_1(t)\, cos(\pi\alpha x) sin(\pi z) + F_2(t)\, sin(2\pi z) \quad (48)$$

$$\varphi = G_1(t)\, sin(\pi\alpha x) cos(\pi z) + G_2(t)\, sin(2\pi z) \quad (49)$$

where, the system dynamics define the amplitudes $D_1(t), E_1(t), F_1(t)$ and $G_1(t)$.

Equating the coefficients of like terms and substituting Equations (46)-(49) into Equations (1)-(7) yields the following nonlinear autonomous system of differential equations.

$$\dot{D}_1 = -V_a\delta^2\eta D_1 - \frac{Ra_T\pi\alpha V_a}{\delta^2}E_1 + \frac{Ra_S\pi\alpha V_a}{\delta^2}F_1 - \pi C_h M_p V_a G_1 \quad (50)$$

$$\dot{E}_1 = -\pi\alpha D_1 - \delta^2 E_1 - \pi^2\alpha D_1 E_2 + QE_1 \quad (51)$$

$$\dot{E}_2 = -4\pi^2 E_2 + \frac{\pi^2\alpha}{2}D_1 E_1 + QE_2 \quad (52)$$

$$\dot{F}_1 = -\pi\alpha D_1 - \delta^2\tau F_1 - \pi^2\alpha D_1 F_2 + \boldsymbol{\chi}E_1 - \boldsymbol{\chi}F_1 \quad (53)$$

$$\dot{F}_2 = -4\pi^2\tau F_2 + \frac{\pi^2\alpha}{2}D_1 F_1 - \boldsymbol{\chi}F_2 + \boldsymbol{\chi}E_2 \quad (54)$$

$$\dot{G}_1 = -M_p(\pi^2\alpha^2 + \pi^2) + \pi G_1 \quad (55)$$

$$\dot{G}_2 = -4\pi^2 M_p G_2 \quad (56)$$

where, the time derivative is represented by the overdot.

The set of Equations (50)-(56) has several characteristics of the entire problem and is uniformly constrained in time. Equations (50)-(56), like the initial Equations (1)-(7), must be dissipative. Therefore, there must be a decrease in volume in space. In order to demonstrate the velocity field has a constant negative divergence volume contraction. Indeed,

$$\frac{\partial\dot{D}_1}{\partial D_1} + \frac{\partial\dot{E}_1}{\partial E_1} + \frac{\partial\dot{E}_2}{\partial E_2} + \frac{\partial\dot{F}_1}{\partial F_1} + \frac{\partial\dot{F}_2}{\partial F_2} + \frac{\partial\dot{G}_1}{\partial G_1} + \frac{\partial\dot{G}_2}{\partial G_2} < 0 \quad (57)$$

Because the right-hand side of Equation (57) is always negative and all physically important parameters are non-negative when enclosed in square brackets, the equation is restricted and dissipative. Equation (57) states that the end points of the relevant trajectories will fill the volume at time $t$ if a set of phase space initial points inhabit the region $V(0)$ at time $t = 0$. This statement is as follows:

$$V(t) = V(0)exp\left[-\left\{\delta^2(\eta V_a + 1 + \tau) + 4\pi^2 + \delta^2 + M_p(\delta^2 + 4\pi^2)\right\}t\right] \quad (58)$$

The set of Equations (50) to (56) is invariant under the symmetry transformation,

$$\left(D_1, E_1, E_2, F_1, F_{2,} G_1, G_{2,}\right) \rightarrow \left(-D_1, -E_1, -E_2, -F_1, -F_{2,} -G_1, -G_{2,}\right).$$

## 7. Finite-amplitude Motions

We investigate the potential for an analytical solution based on qualitative predictions. Equations (50)-(56) can be solved using closed form for steady motions. Left-hand sides of Equations (50)-(56) are equal to zero, and the result is:

$$-V_a\delta^2\eta D_1 - \frac{Ra_T\pi\alpha V_a}{\delta^2}E_1 + \frac{Ra_S\pi\alpha V_a}{\delta^2}F_1 - \pi C_h M_p V_a G_1 = 0 \quad (59)$$

$$-\pi\alpha D_1 - \delta^2 E_1 - \pi^2\alpha D_1 E_2 + QE_1 = 0 \quad (60)$$

$$-4\pi^2 E_2 + \frac{\pi^2\alpha}{2}D_1 E_1 + QE_2 = 0 \quad (61)$$

$$-\pi\alpha D_1 - \delta^2\tau F_1 - \pi^2\alpha D_1 F_2 + \chi E_1 - \chi F_1 = 0 \quad (62)$$

$$-4\pi^2\tau F_2 + \frac{\pi^2\alpha}{2} D_1 F_1 - \chi F_2 + \chi E_2 = 0 \quad (63)$$

$$-M_p(\pi^2\alpha^2 + \pi^2) + \pi G_1 = 0 \quad (64)$$

$$-4\pi^2 M_p G_2 = 0 \quad (65)$$

By removing all coefficients between Equations (59)-(65) other than $D_1$, we obtain:

$$a_1 x^2 + b_1 x + c_1 = 0 \quad (66)$$

where, $x = \frac{D_1^2}{8}$, $a_1 = \eta\delta^2\alpha^4 c(\alpha^2 + \pi^2)$,

$$b_1 = \frac{\eta\delta^4\alpha^2(4\pi^2+\chi)}{\pi^2}(1+\tau^2)(\pi^2+Q) + \frac{\alpha^4(\pi^2+Q)}{\delta^2}(4\pi^2+\chi)(\tau Ra_S - Ra_T),$$

$$c_1 = \frac{\eta\delta^6\tau^2(\pi^2+Q)(4\pi^2+\chi)}{\pi^4} + \frac{\tau^2\alpha^2(4\pi^2+\chi)}{\pi^2}\left(\frac{Ra_S}{\tau} + Ra_T\right)(\pi^2+Q)$$

and $\delta^2 = \pi^2(\alpha^2+1)$.

We have an expression for $Ra_T^f$ (the finite-amplitude Rayleigh number) which indicates the beginning of steady movements of finite-amplitude, by allowing the radical in the solution of Equation (66) to disappear. The formula for the finite-amplitude Rayleigh number is

$$Ra_T^f = \frac{1}{2x_1}\left\{-x_2 + (x_2^2 - 4x_1x_3)^{(1/2)}\right\} \quad (67)$$

where,

$$x_1 = \frac{\alpha^8}{\delta^4},$$

$$x_2 = \frac{4\eta\delta^2\alpha^6\tau^2(\pi^2+Q)(4\pi^2+\chi)}{\pi^2} - \frac{2\eta\delta^2\alpha^6(4\pi^2+\chi)(1+\tau^2)(\pi^2+Q)}{\pi^2} - \frac{2\alpha^8\tau Ra_S(4\pi^2+\chi)(\pi^2+Q)}{\delta^4},$$

$$x_3 = \frac{\eta^2\delta^8\alpha^4}{\pi^4}(4\pi^2+\chi)(1+\tau^2+\tau^4)(\pi^2+Q) + \frac{\alpha^8\tau^2 Ra_S^2(\pi^2+Q)(4\pi^2+\chi)}{\delta^4} + \frac{2\eta\delta^2\alpha^6\tau(4\pi^2+\chi)(1+\tau^2)(\pi^2+Q)Ra_S}{\pi^2} - \frac{4\eta\delta^2\tau\alpha^6 Ra_S(\pi^2+Q)(4\pi^2+\chi)}{\pi^2}$$

In order to determine the initial impact in the situation of finite-amplitude convection, an analytical statement for the finite-amplitude Rayleigh number is obtained by applying Equation (67), which numerically minimizes a set of physical parameter values with regard to the wavenumber.

## 8. Heat and Mass Transport

In order to fully understand convection due to heat and mass transport phenomena in fluids, measurements of heat and mass transfer are essential. This is because the effects of convection on heat and mass transmission become more pronounced as the Rayleigh number increases. Only in the initial state mass and heat can be transferred by conduction.

If the rates of heat and mass transmission per unit area are $H$ and $J$, respectively, then

$$H = -\kappa_T \left\langle \frac{\partial T_{total}}{\partial z} \right\rangle_{z=0} \quad (68)$$

$$J = -\kappa_S \langle \frac{\partial S_{total}}{\partial z} \rangle_{z=0} \tag{69}$$

where, a horizontal average is shown by the angular bracket and

$$T_{total} = T_0 - \Delta T \frac{z}{d} + T(x,z,t) \tag{70}$$

$$S_{total} = S_0 - \Delta S \frac{z}{d} + S(x,z,t) \tag{71}$$

Equations (47) and (48), respectively, are substituted into Equations (70) and (71), and using the resulting Equations in (70) and (71), we get,

$$H = \frac{\kappa_T \Delta T}{d}(1 - 2\pi E_2) \tag{72}$$

$$J = \frac{\kappa_S \Delta S}{d}\left[(1 - 2\pi F_2) + \frac{Ra_T}{Ra_S}(1 - 2\pi E_2)\right] \tag{73}$$

The definitions of the Nusselt and Sherwood numbers are

$$Nu = \frac{H}{\kappa_T \Delta T/d} = 1 - 2\pi E_2 \tag{74}$$

$$Sh = \frac{J}{\kappa_S \Delta T/d} = \left[(1 - 2\pi F_2) + \frac{Ra_T}{Ra_S}(1 - 2\pi E_2)\right] \tag{75}$$

Writing $E_2$ and $F_2$ in terms of $D_1$, using Equations (59)-(65), and substituting in Equations (74) and (75), respectively, we obtain Equations (59)-(65) and Equations (74) and (75), respectively, are used to write $E_2$ and $F_2$ in terms of $D_1$.

$$Nu = 1 + \frac{2\pi^2\alpha^2\chi}{\lambda\pi^2\alpha^2 + \pi^2(1+\alpha^2\chi)} \tag{76}$$

$$Sh = 1 - 2\pi\left[\frac{\pi\alpha^2 Ra_T\chi}{Ra_S(\lambda\pi^2\alpha^2 + \pi^2 + \pi^2\alpha^2\chi)} - \left\{\frac{\pi\alpha^2\chi}{\pi^2 + \pi^2\alpha^2(1+\chi)}\right\}\left\{1 - \frac{\pi^2(1+\alpha^2)Ra_T}{Ra_S(\lambda\pi^2\alpha^2 + \pi^2 + \pi^2\alpha^2\chi)} + \frac{\pi^2\alpha^2 Ra_T\chi}{Ra_S(\lambda\pi^2\alpha^2 + \pi^2 + \pi^2\alpha^2\chi)}\right\}\right] + \frac{Ra_T}{Ra_S}\left[1 + \frac{2\pi^2\alpha^2\chi}{(\lambda\pi^2\alpha^2 + \pi^2 + \pi^2\alpha^2\chi)}\right] \tag{77}$$

Contribution of convection to heat and mass transmission is shown by the second term in Equations (76) and (77), respectively, on the right-hand side.

## 9. Results and Discussion

The present study illustrates the influence of magnetoconvection on thermal and solutal buoyancy forces with inclusion of couple stress fluid. There are distinguished physical situations taken into account. A validation of the obtained results is provided below before going into the impact of various parameters on the physical problem that is being presented. Here **Table 1** and **Table 2** are presented as a comparison of results in a special case in absence of hydromagnetic convection compared with published results of Malashetty et al. (2010):

**Table 1.** Comparative values of the critical solute Rayleigh number for various values of the diffusivity ratio, couple-stress parameter and Vadasz number during stationary mode convention by Malashetty et al. (2010).

| $\tau$ | $C$ | $Va$ | $Ra_S^*$ Malashetty et al. (2010) | $Ra_S^*$ (Present Study) |
|---|---|---|---|---|
| 0.3 | 1.0 | 1.0 | 39.80 | 39.80 |
| 0.5 | 1.0 | 1.0 | 316.20 | 316.20 |
| 0.7 | 1.0 | 1.0 | 1995.00 | 1995.00 |

**Table 2.** Comparative values of the critical thermal Rayleigh number for various values of the diffusivity ratio, couple-stress parameter and Vadasz number during oscillatory mode by Malashetty et al. (2010).

| $\tau$ | $C$ | $Va$ | $Ra_{T_c}^{osc}$ Malashetty et al. (2010) | Present Value of $Ra_{T_c}^{osc}$ |
|---|---|---|---|---|
| 0.3 | 1.0 | 1.0 | 1031.0 | 1031.0 |
| 0.5 | 1.0 | 1.0 | 2205.0 | 2205.0 |
| 0.7 | 1.0 | 1.0 | 2264.0 | 2264.0 |

Here **Table 3** is presented as a Comparison of asymptotic $(A)$ and exact $(E)$ values of the critical Rayleigh number $(R_c)$ and the critical wave number $(a_c)$ for different values of $H$ with $Da^{-1} = 100$ and $\gamma = 1$ with published results of Shivakumara et al. (2016).

**Table 3.** Comparison of asymptotic $(A)$ and exact $(E)$ values of the critical Rayleigh number $(R_c)$ and the critical wave number $(a_c)$ for different values of $H$ with $Da^{-1} = 100$ and $\gamma = 1$ with published results of Shivakumara et al. (2016).

| $Q$ | $\log_{10} H$ | $R_c(A)$ | $a_c(A)$ | $R_c(E)$ Shivakumara et al. (2016) | $R_c(E)$ (Present Study) | $a_c(E)$ Shivakumara et al. (2016) | $a_c(E)$ (Present Study) |
|---|---|---|---|---|---|---|---|
| 0 | -1.0 | 4724.49 | 2.929 | 4724.5 | 4724.5 | 2.929 | 2.929 |
| 0 | 0.0 | 4935 | 2.978 | 4939.18 | 4939.18 | 2.978 | 2.978 |
| 0 | 1.0 | 5922.7 | 2.582 | 6316.63 | 6316.63 | 1.448 | 1.448 |
| 100 | -1.0 | 6684.32 | 3.409 | 6684.32 | 6684.32 | 3.409 | 3.409 |
| 100 | 0.0 | 6686.44 | 3.466 | 6947.05 | 6947.05 | 3.466 | 3.466 |
| 100 | 1.0 | 6742.14 | 3.124 | 8706.91 | 8706.91 | 3.686 | 3.686 |
| 1000 | -1.0 | 20,382.8 | 4.969 | 20,382.8 | 20,382.8 | 4.969 | 4.969 |
| 1000 | 0.0 | 20,889.2 | 5.053 | 20,889.7 | 20,889.7 | 5.054 | 5.054 |
| 1000 | 1.0 | 24,526.8 | 4.937 | 24,644.0 | 24,644.0 | 5.472 | 5.472 |

Here **Table 4** is presented as a comparison of asymptotic $(A)$ and exact $(E)$ values of the critical Rayleigh number $(Ra_c)$ and the critical wave number $(a_c)$ for different values of $H$ with $Da^{-1} = 100$ and $\gamma = 1$ with published results of Shivakumara et al. (2016).

**Table 4.** Evaluation of $Ra_{Tc}^{sc}$ and $Ra_{Tc}^{oc}$ for different values of $S_h$ and C when for stationary $Ta = 800, Le = 5$ and $Ra_s = 500$ for oscillatory $Ta = 1200, Le = 5, Ra_s = 500$, and $Pr = 0.9$ with published results of Nagaraju et al. (2023).

| | Stationary $Ra_{Tc}^{sc}$ | | Oscillatory $Ra_{Tc}^{oc}$ | |
|---|---|---|---|---|
| $S_h$ | $C$ = 0.29 Nagaraju et al. (2022) | $C$ = 0.29 (Present Study) | $C$ = 0.29 Nagaraju et al. (2022) | $C$ = 0.29 (Present Study) |
| 1 | 6238.8892 | 6238.8892 | 5292.7653 | 5292.7653 |
| 2 | 6235.9628 | 6235.9628 | 5289.7445 | 5289.7445 |
| 3 | 6227.1798 | 6227.1798 | 5280.6123 | 5280.6123 |

The flow dynamics and stability analysis under many physical parameters those are responsible for the instability of a chemically reacting couple-stress fluid in a saturated porous layer are thoroughly studied in this section. We fixed a small number of factors throughout the entire investigation to lessen the impact of specific physical elements on stability. The range of additional controlling factors is chosen depending on how this sort of problem is used in practice. The conventional normal mode analysis and the Fourier series expansion strategy are utilized in the linear theory of stability mechanism. The stationary and oscillatory modes in relation to Rayleigh numbers are calculated and graphically presented for a range of parameter values, including the heat source, chemically reactive parameter, diffusivity ratio, couple-stress parameter and solute Rayleigh number.

**Figure 2** shows the influence of the solute Rayleigh number $Ra_s$ at the values $V_a = 1, Q = 1.5, \chi = 0.4, C = 3, M_p = 10^{-3}, C_h = 10$. This graph shows that as $Ra_s$ is raised, the least value of Rayleigh number in stationary mode decreases. This demonstrates how the solute Rayleigh number stabilizes the dynamics of the flow.

**Figure 3** demonstrates that the minimum Rayleigh number for both stationary and oscillatory modes rise as the solute Rayleigh number increases, suggesting a stabilizing influence, which has a quite similar effect in **Figure 2** geometrically.

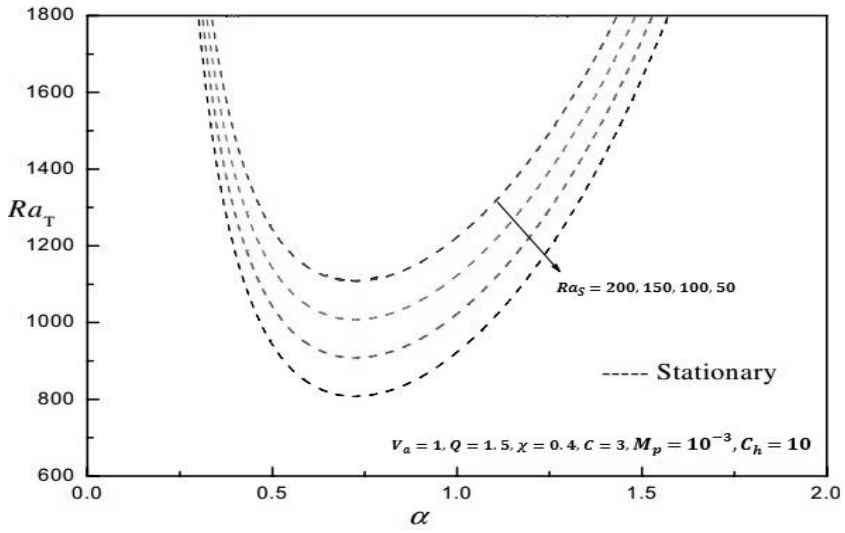


**Figure 2.** Curves showing neutral stability for various values of $Ra_s$.

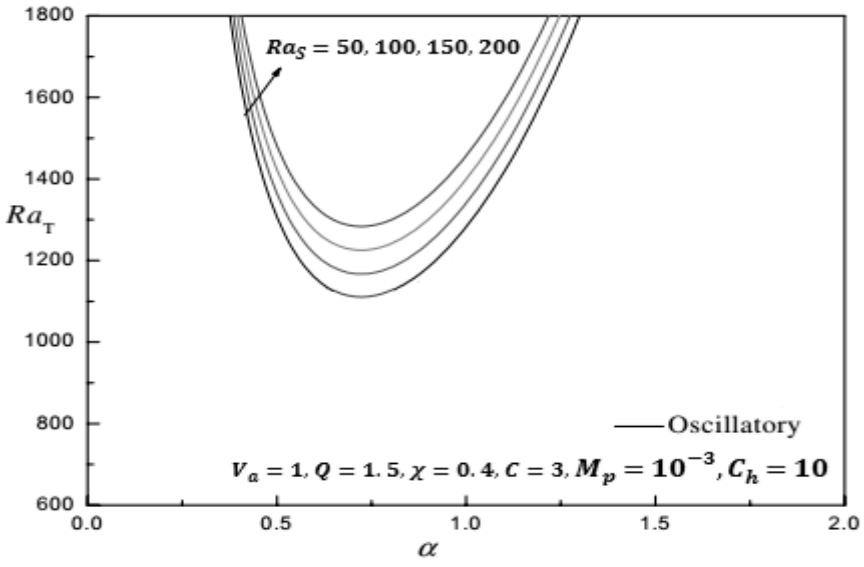


**Figure 3.** Curves showing neutral stability for various values of $Ra_s$.

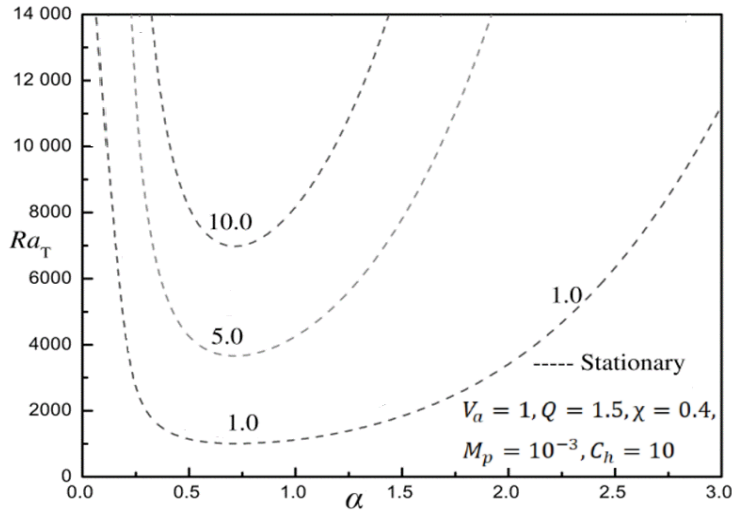


**Figure 4.** Curves illustrating neutral stability for various couple stress parameter values $(C)$.

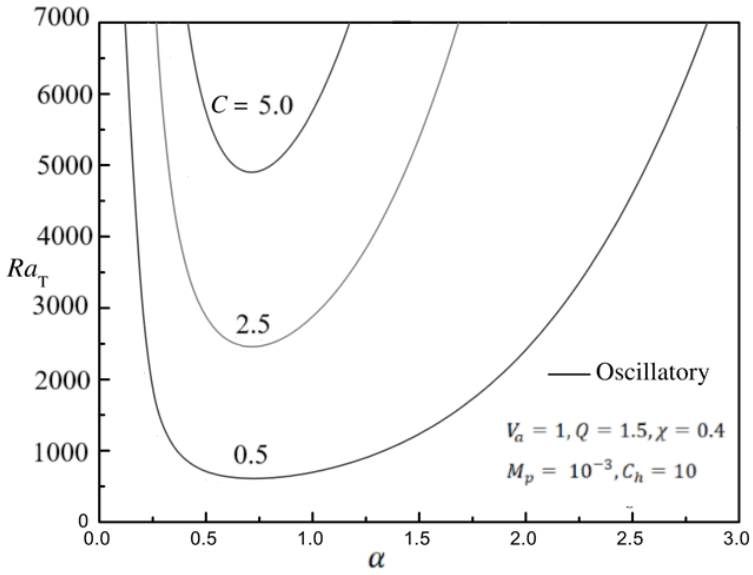


**Figure 5.** Variation of Rayleigh number and $\alpha$ (the wave number) for neutral stability curves for the couple stress parameter $(C)$.

The neutral stability curves are shown in **Figure 4** and **Figure 5** for the couple-stress parameter change with the following other parameters: $V_a = 1, Q = 1.5, \chi = 0.4, Ra_S = 10^2, M_p = 10^{-3}, C_h = 10$. The minimal value of the Rayleigh number for both stationary and oscillatory modes increases as the couple-stress parameter C is increased, as these graphs demonstrate, proving that the couple-stress parameter stabilizes the system for fixed values of $V_a = 1, Q = 1.5, C = 5, Ra_S = 10^2, M_p = 10^{-3}, C_h = 10$. This suggests that the couple-stress parameter has a stabilizing effect on the system, which is identical to the result in **Figure 4** geometrically.

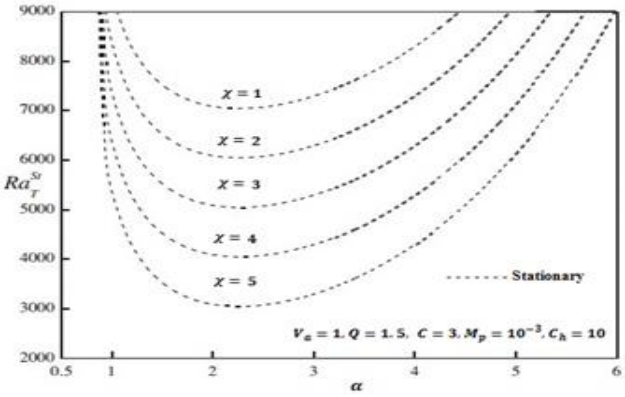


**Figure 6.** Curves for neutral stability for various values of the chemical reaction parameter $(\chi)$.

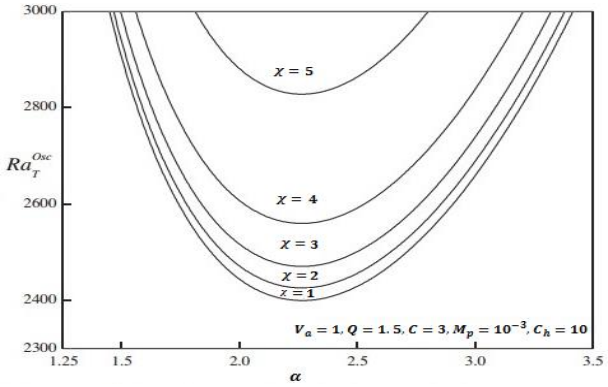


**Figure 7.** Curves illustrating neutral stability for various values in chemical reaction parameter $(\chi)$.

**Figure 6** and **Figure 7** illustrate how the solute chemical reaction parameter, $\chi$, affects the neutral stability curves for both oscillatory and stationary modes. This graph demonstrates how the lowest Rayleigh number for both the stationary and oscillatory modes increase with an increase in the chemical reaction parameter $\chi$, indicating a stabilizing effect.

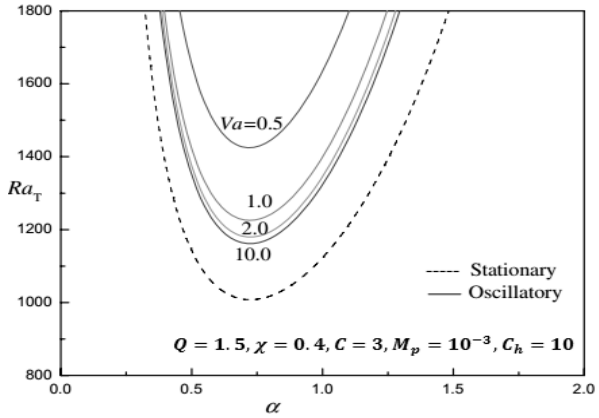


**Figure 8.** Curves showing neutral stability for various values of the Vadasz number $(V_a)$.

For the following values, **Figure 8** shows how the Vadasz number affects the neutral curves of oscillatory mode: $Q = 1.5, \chi = 0.4, C = 5, Ra_S = 10^2, M_p = 10^{-3}, C_h = 10$. The oscillatory Rayleigh number is found to decrease as the Vadasz number rises, demonstrating that in the situation of oscillatory convection, the Vadasz number destabilizes the system.

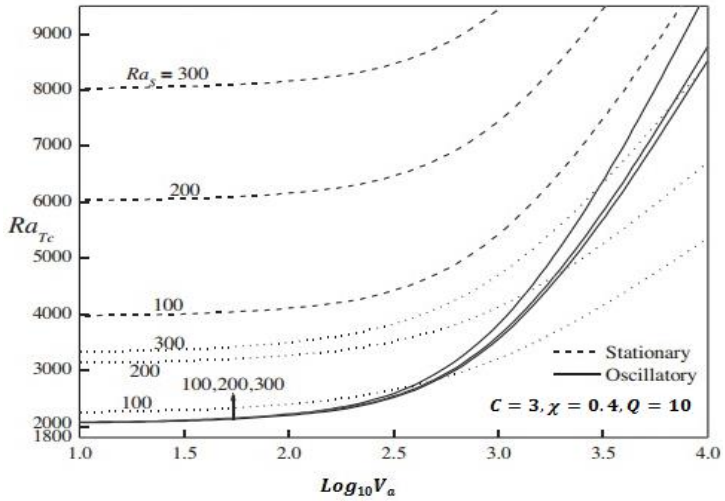


**Figure 9.** Variation of critical Rayleigh number with Vadasz $V_a$ for Various values of $Ra_s$.

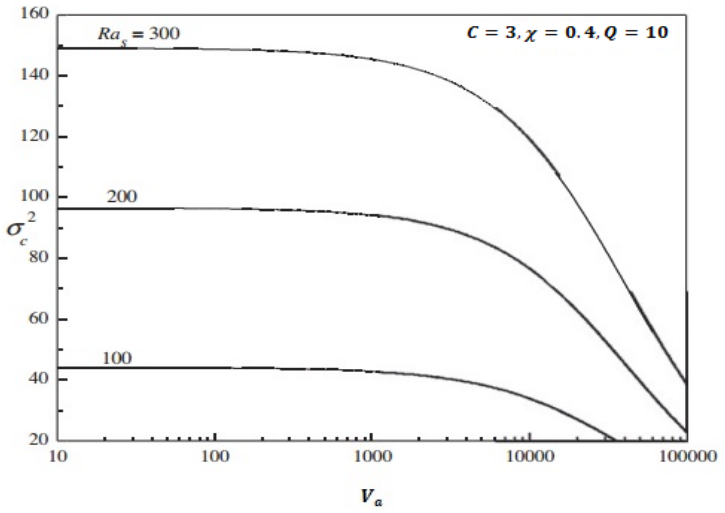


**Figure 10.** Critical frequency varies with Vadasz $V_a$ for various values of $Ra_s$.

For a range of solute Rayleigh number values, **Figure 9** and **Figure 10** show the oscillation of the critical stationary and oscillatory Rayleigh numbers as well as the critical frequency of the oscillatory mode. As the solute Rayleigh number grows, so does the critical Rayleigh number for stationary, oscillatory, and finite amplitude modes, which improves the stability of the system, as can be shown in **Figure 9** and **Figure 10**.

The critical frequency of the oscillatory mode with the Vadasz number for different values of the couple stress parameter $C$, as well as the fluctuation of the critical Rayleigh number for stationary, oscillatory, and finite amplitude modes, are depicted in **Figure 11** and **Figure 12**. These values are $\chi = 0.4, Q = 1.5$, $Ra_S = 10^2, M_p = 10^{-3}, C_h = 10$. We can see from this figure that, while the Vadasz number is kept fixed, the couple stress parameter stabilizes the system since the critical Rayleigh number for stationary, oscillatory and finite amplitude modes increases with increasing couple stress parameter $C$. **Figure 12** shows the impact of the couple stress parameter $C$ on the critical frequency. The figure shows a clear decrease in frequency with a rise in the couple stress parameter, whereas large values of frequency are specifically associated to small values of $V_a$ and decrease as $V_a$ increases.

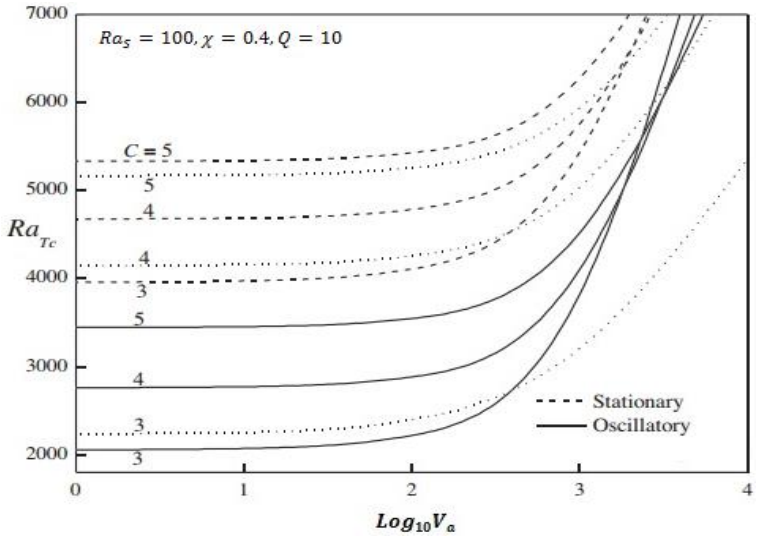


**Figure 11.** Variation of the Vadasz number $V_a$ and $R_{Tc}$(critical Rayleigh number) for various values of $C$.

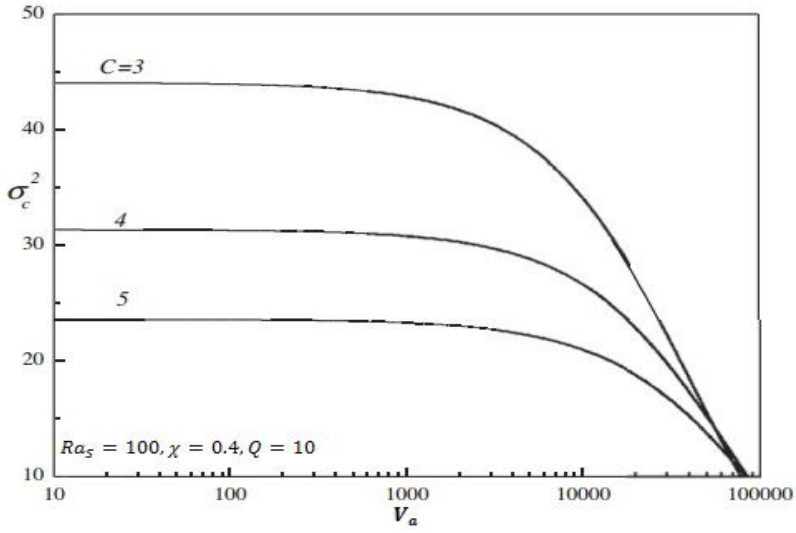


**Figure 12.** Critical frequency variation with respect to the Vadasz number $V_a$ for various values of $C$.

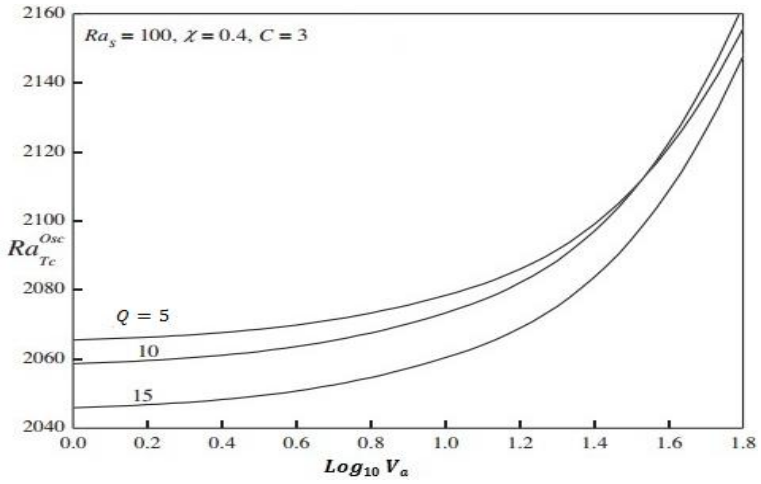


**Figure 13.** Critical Rayleigh number's variation with Vadasz number $V_a$ for various values of $Q$.

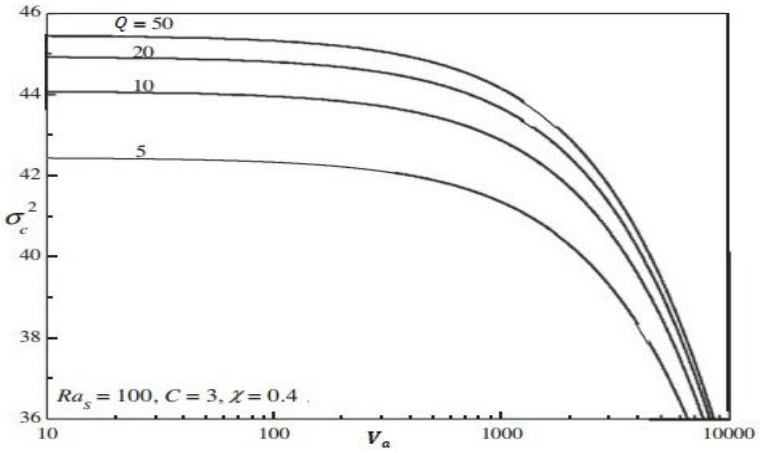


**Figure 14.** Variation of the critical frequency for different values of Q with the Vadasz number $V_a$.

The fluctuation of the critical Rayleigh number for oscillatory mode and the critical frequency with Vadasz number for various values of the heat source parameter Q is shown in **Figure 13** and **Figure 14**. As the value of the heat source parameter Q increases, the critical oscillatory Rayleigh number lowers, which suggests that the heat source parameter Q facilitates the beginning of oscillatory convection, as seen in **Figure 13** and **Figure 14**. Furthermore, it is discovered that as Q is increased, the critical frequency rises as well. In this case, the heat source acts as a destabilizing element. Additionally, we discover that the couple-stress parameter has negligible effect for large solute Rayleigh numbers. In **Figure 13** and **Figure 14**, when the Vadasz number and couple-stress parameter are fixed, the diffusivity ratio $\tau$ has a dual influence on the oscillatory mode, as indicated by the trend reverting after a certain value of $Ra_s$. The critical Rayleigh number of the oscillatory mode varies with varying Vadasz numbers. The critical oscillatory Rayleigh number falls as the Vadasz number increases, which suggests that the Vadasz number precedes the commencement of oscillatory convection.

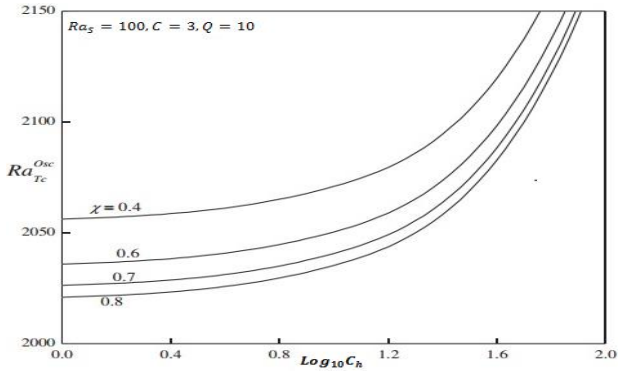


**Figure 15.** Variation of critical Rayleigh number with Chandrasekhar number $C_h$ for various $\chi$ values.

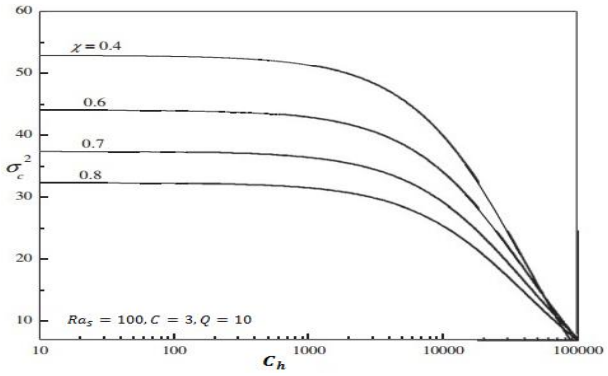


**Figure 16.** Variation of critical frequency with Chandrasekhar number $C_h$ for various values of $\chi$.

**Figure 15** and **Figure 16** on the $(Ra_{Tc}, C_h)$ plane show the influence of the chemical reaction parameter $\chi$ on the critical oscillatory Rayleigh number and critical frequency. We discover that increasing the value of $C_h$ lowers the essential Rayleigh number for oscillatory mode, and as chemical responding parameter increases, the thermal-solutal 'lag' effect occurs and is decreased. This increases the efficiency of heat transmission and facilitates the production of convection by the destabilizing thermal buoyancy gradient. With the chemical reaction, the critical frequency falls (see **Figure 16**).

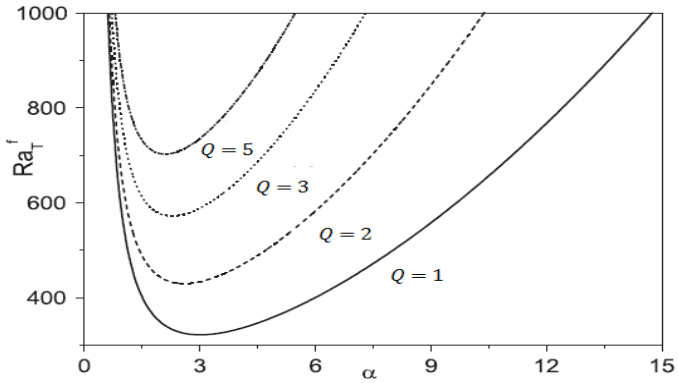


**Figure 17.** Variation of Rayleigh number with a finite amplitude and $\alpha$ (the wave number) for various values of $Q$ and for $V_a = 10, C = 2,\ M_p = 10^{-3}, C_h = 10, Ra_s = 50$.

A quantitative analysis of the convective heat and mass transport over the porous layer is done, and the results of the weakly nonlinear theory are provided. While the other parameters Q, $\xi$, $\eta$, Le, $M_p$ , $C_h$ and $\lambda$ are kept at 1, 1, 1, 0.5, $10^{-3}$, 10, and 0.7 correspondingly, we have calculated the Nusselt number (Nu) and Sherwood number (Sh). For the unique value of the heat source parameter Q, the fluctuation of the finite-amplitude on Rayleigh number with wave number is shown in **Figure 17** for $V_a = 10,\ C = 2, \chi = 0.4,\ and\ Ra_s = 50$. Here, we have seen that the profile abruptly decreases while $0.5 < \alpha < 2.5$ for all values of Q. After then, it keeps steadily rising. Additionally, it is noted that with greater values of Q, the highest possible magnitude of finite amplitude increases. These phenomena distinguish between oscillatory and stationary convection.

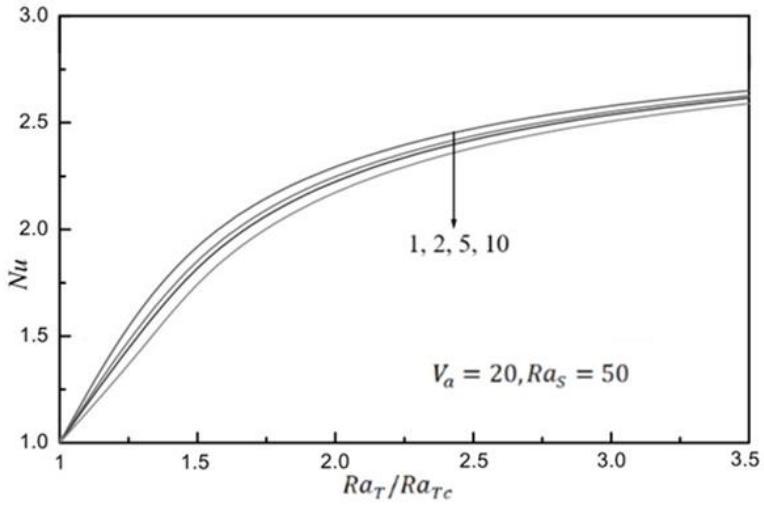


**Figure 18.** Variations of Nusselt number and critical Rayleigh number for various values of $Ra_S$.

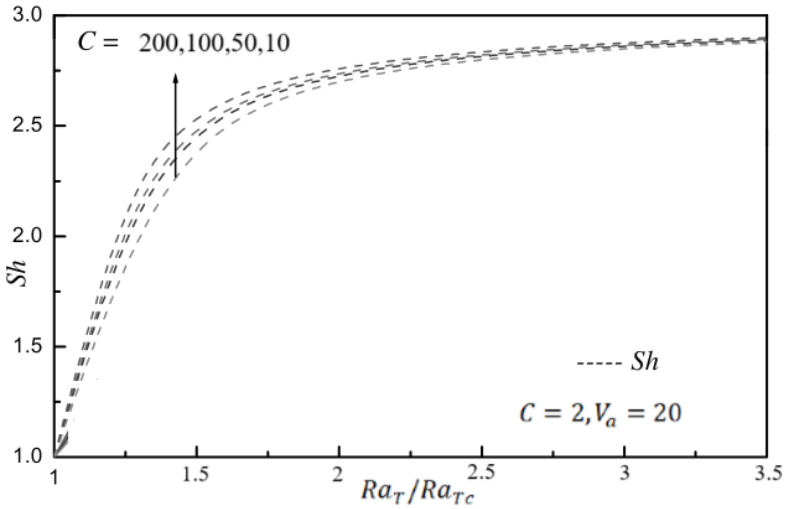


**Figure 19.** Variations of Sherwood number and critical Rayleigh number for various values of $Ra_S$.

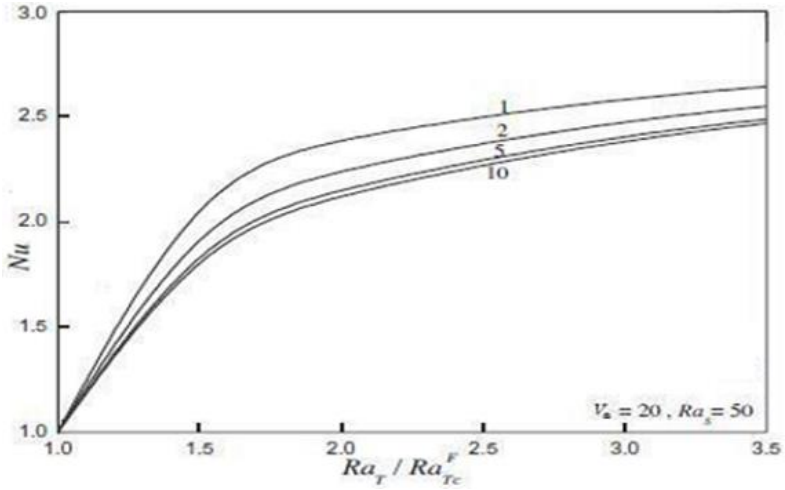


**Figure 20.** Variation of Nusselt number with critical Rayleigh number for various values of $C$.

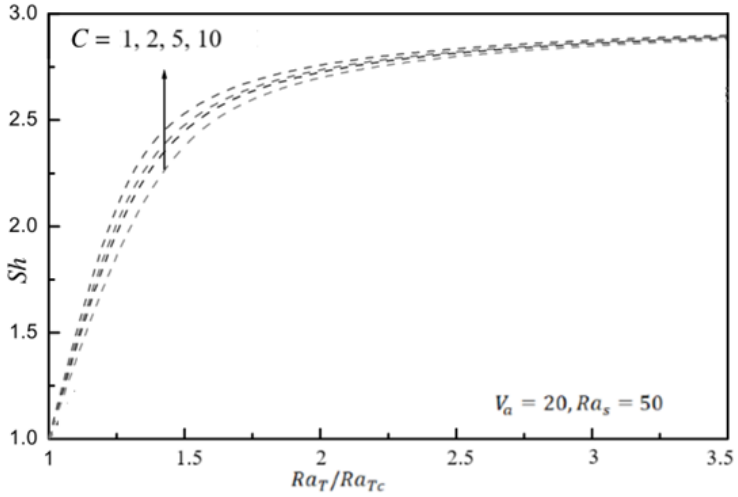


**Figure 21.** Variation of Sherwood number with $R_{Tc}$(critical Rayleigh number) for various values of $C$.

The determination of mass and heat transfer across the layer is crucial to the study of double-diffusive convection. In order to comprehend the fluctuation of convective transfer of heat and mass in the research of double diffusive convection at $V_a = 10,\ C = 2, \chi = 0.4,\ Ra_s = 50$, **Figure 18** and **19** are plotted. These numbers show that the beginning of convection is more effective in raising the Rayleigh number. Nu and Sh, which indicate the ratio of heat or mass transmitted across the layer to the heat or mass conveyed by conduction, respectively, give the rate of heat and mass transfer throughout the layer. The variation in the rate of the transfer of heat and mass for the selected value of the couple stress parameter $C$ at $V_a = 20$ is shown in **Figure 20** and **Figure 21**. These numbers show that as the value of $C$ is raised, the rate of heat transmission falls. However, in the event of mass transfer, no noteworthy change is mentioned. The impact of different parameters on Sherwood number $Sh$ and Nusselt number $Nu$ is shown in **Figures 18-21**.

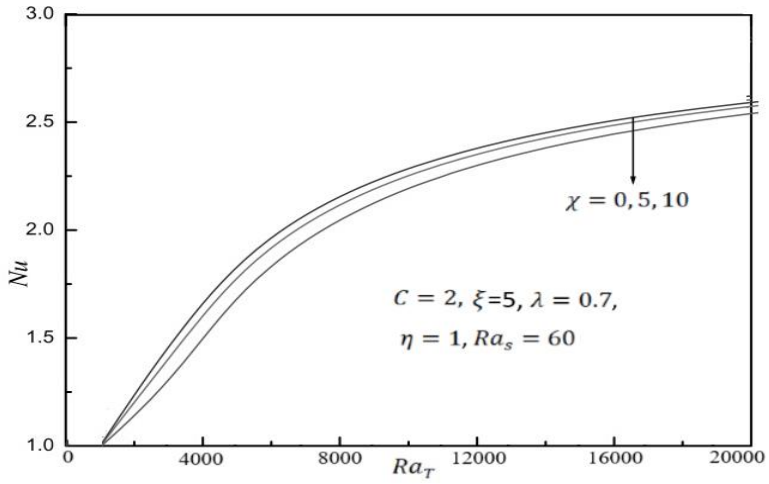


**Figure 22.** Variation of Nusselt number with Rayleigh number $Ra_T$ for various values of $\chi$.

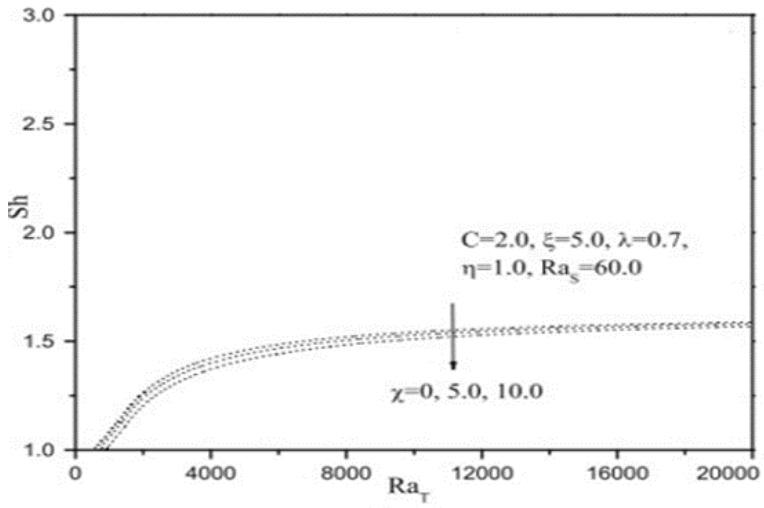


**Figure 23.** Variation of Sherwood number with Rayleigh number $Ra_T$ for various values of $\chi$.

It is also found that the value of $Ra_T$ is increased beyond its critical value. Additionally, it is discovered that the transportation of mass and heat increases asymptotically as $Ra_T$ is raised above its critical value, continuing until $Ra_T$ reaches a certain threshold. However, the value of $Ra_T$ rises. In addition to this, it is discovered in **Figure 22** and **23** that as C increase, both heat and mass transmission decrease. As a result, convection has substantial degradation. However, $Nu$ and $Sh$ become nearly constants as $Ra_T$ is raised much higher. Additionally, it is discovered from **Figure 22** and **23**, respectively, that mass and heat transfers decrease as $C$ and $\chi$ increase. Convection thus occurs with a delay.

## 10. Conclusions

The onset of magnetoconvective double-diffusive convection within a couple-stress fluid-saturated the horizontal porous layer, is examined using linear and weakly nonlinear stability analysis mechanism. The

modified Darcy equation, which incorporates the inertia element in the time derivative term, is utilized to model the momentum equation. The distinguished equations for the stationary and oscillatory mode convection and finite-amplitude Rayleigh numbers are obtained as functions of the governing parameters. The effects of stationary, oscillatory, finite-amplitude convection, a heat source, a couple stress parameter, a solute Rayleigh number and a Vadasz number are shown on a graph. The following are the conclusions:

- The solute Rayleigh number parameter stabilizes the stationary as well as the oscillatory convection.
- The couple-stress parameter is also having a stabilizing effect on the distinguished state of convection.
- The solute Rayleigh number parameter is also having stabilizing property for the finite amplitude convection.
- The Vadasz number indicates that it has a destabilizing effect since it moves the onset of oscillatory convection forward.
- Heat Source parameter Q accelerates the beginning of oscillatory convection.
- Convection is created when the thermal buoyancy gradient is unstable due to the chemical reaction parameter $\chi$.
- A couple-stress linearly heated fluid with a saturated horizontal porous layer beneath a magnetic field is the subject of an analysis for weak nonlinear stability.
- The momentum equation uses the modified Darcy equation, the inertia term, and the magnetic field as inputs. For the representation of the stream function $\psi$, temperature $T$, and concentration $S$, a Fourier series is used.
- Both the solute Rayleigh number and the couple-stress parameter stabilize finite-amplitude convection.
- The rate of heat and mass transfer reduces with increasing couple-stress parameter $C$, while both rates rise with increasing solute Rayleigh number $Ra_S$.

**Conflict of Interest**
There are no conflicts of interest to disclose in connection with this publication.

**Acknowledgments**
The authors wish to express their gratitude to the editor and the anonymous reviewers of the journal.

## References

Alchaar, S., Vasseur, P., & Bilgen, E. (1995a). Effects of a magnetic field on the onset of convection in a porous medium. *Heat and Mass Transfer, 30*, 259-267.

Alchaar, S., Vasseur, P., & Bilgen, E. (1995b). Hydromagnetic natural convection in a tilted rectangular porous enclosure. *Numerical Heat Transfer, Part A: Applications*, *27*(1), 107-127.

Barletta, A., & Rees, D.A.S. (2019). On the onset of convection in a highly permeable vertical porous layer with open boundaries. *Physics of Fluids*, *31*, 074106.

Bharty, M., Srivastava, A.K., & Mahato, H. (2023). Stability of magneto double diffusive convection in couple stress liquid with chemical reaction. *Journal of Heat and Mass Transfer Research*, *10*(2), 171-190.

Bharty, M., Srivastava, A.K., & Mahato, H. (2024). The effect of chemical reaction on thermo-solutal magneto-convection under non-equilibrium temperature conditions. *International Journal of Advances in Engineering Sciences and Applied Mathematics*, 16, 256-267.

Bian, W., Vasseur, P., & Bilgen, E. (1996a). Effect of an external magnetic field on buoyancy-driven flow in a shallow porous cavity. *Numerical Heat Transfer, Part A Applications*, *29*(6), 625-638.

Bian, W., Vasseur, P., Bilgen, E., & Meng, F. (1996b). Effect of an electromagnetic field on natural convection in an inclined porous layer. *International Journal of Heat and Fluid Flow*, *17*(1), 36-44.

Chandrasekhar, S. (1981). *Hydrodynamics and hydromagnetic stability*. Dover Publications, New York.

Chang, M.H., & Chen, C.O.K. (1998). Hydromagnetic stability of current-induced flow in a small gap between concentric rotating cylinders. *Proceedings of the Royal Society of London. Series A: Mathematical, Physical and Engineering Sciences*, *454*(1975), 1857-1873.

Chen, C., & Lai, D. (2010). Weakly nonlinear stability analysis of a thin magnetic fluid during spin coating. *Mathematical Problem in Engineering*, *2010*, 1-17.

Choudhary, S. (2019). Global stability for double-diffusive convection in a couple-stress fluid saturating a porous medium. *Studia Geotechnica et Mechanica*, *41*(1), 13-20.

Choudhary, S., Choudhary, P., Alessa, N., & Loganathan, K. (2023). MHD thermal and solutal stratified stagnation flow of tangent hyperbolic fluid induced by stretching cylinder with dual convection. *Mathematics*, *11*(9), 2182. https://doi.org/10.3390/ math11092182.

Drazin, P.G. (2012). *Introduction to hydrodynamics stability*. Cambridge University Press, U.K.

Gaikwad, S.N., Malashetty, M.S., & Prasad, K.R. (2009a). An analytical study of linear and nonlinear double diffusive convection in a fluid saturated anisotropic porous layer with Soret effect. *Applied Mathematical Modelling*, *33*(9), 3617-3635.

Gaikwad, S.N., Malashetty, M.S., & Prasad, K.R. (2009b). Linear and non-linear double diffusive convection in a fluid-saturated anisotropic porous layer with cross-diffusion effects. *Transport in Porous Media*, *80*, 537-560.

Harfash, A.J., & Meften, G.A. (2018). Couple stresses effect on linear instability and nonlinear stability of convection in a reacting fluid. *Chaos, Solitons & Fractals*, *107*, 18-25.

Herdrich, G., Auweter-Kurtz, M., Fertig, M., Nawaz, A., & Petkow, D. (2006). MHD flow control for plasma technology applications. *Vacuum*, *80*(11-12), 1167-1173.

Jang, J., & Lee, S.S. (2000). Theoretical and experimental study of MHD (magnetohydrodynamic) micropump. *Sensors and Actuators A: Physical*, *80*(1), 84-89.

Kaloni, P.N., & Lou, J.X. (2002). On the stability of thermally driven shear flow of an Oldroyd-B fluid heated from below. *Journal of Non-Newtonian Fluid Mechanics*, *107*(1-3), 97-110.

Kim, M.C., & Cardoso, S.S. (2018). Diffusivity ratio effect on the onset of the buoyancy-driven instability of an A+ B→ C chemical reaction system in a Hele-Shaw cell: Asymptotic and linear stability analyses. *Physics of Fluids*, *30*, 094102.

Kumar, G., Narayana, P.A.L., & Sahu, K.C. (2020). Linear and nonlinear thermosolutal instabilities in an inclined porous layer. *Proceedings of the Royal Society A*, *476*(2233), 20190705.

Mahajan, A., & Nandal, R. (2017). On the stability of penetrative convection in a couple-stress fluid. *International Journal of Applied and Computational Mathematics*, *3*, 3745-3758.

Mahajan, A., & Tripathi, V.K. (2021). Stability of a chemically reacting double-diffusive fluid layer in a porous medium. *Heat Transfer*, *50*(6), 6148-6163.

Malashetty, M.S., & Kollur, P. (2011). The onset of double diffusive convection in a couple stress fluid saturated anisotropic porous layer. *Transport in Porous Media*, *86*, 435-459.

Malashetty, M.S., Pal, D., & Kollur, P. (2010). Double-diffusive convection in a Darcy porous medium saturated with a couple-stress fluid. *Fluid Dynamics Research*, *42*, 035502.

Mendis, R.L.A., Sekimoto, A., Okano, Y., Minakuchi, H., & Dost, S. (2020). Global linear stability analysis of thermo-solutal Marangoni convection in a liquid bridge under zero gravity. *Microgravity Science and Technology*, *32*, 729-735.

Mishra, P., Reddy, Y.D., Goud, B.S., Kumar, D., & Singh, P.K. (2022). Study on linear and nonlinear stability analysis of double diffusive electro-convection in couple stress anisotropic fluid-saturated rotating porous layer. *Journal of the Indian Chemical Society*, *99*(9), 100611.

Muyinda, N., De Baets, B., & Rao, S. (2018). On the linear stability of some finite difference schemes for nonlinear reaction-diffusion models of chemical reaction networks. *Communications in Applied and Industrial Mathematics*, *9*(1), 121-140.

Nagaraju, J., Babu, K.R., Reddy, G.S.K., & Ragoju, R. (2023). On oscillatory rotating convection of a couple-stress fluid with helical force. *Heat Transfer*, *52*(3), 2576-2592.

Nandal, R., & Mahajan, A. (2018). Penetrative convection in couple-stress fluid via internal heat source/sink with the boundary effects. *Journal of Non-Newtonian Fluid Mechanics*, *260*, 133-141.

Nield, D.A., & Bejan, A. (2006). *Convection in porous media* (Vol. 3, pp. 629-982). Springer, New York.

Patil, P.R., & Rudraiah, N. (1973). Stability of hydromagnetic thermoconvective flow through porous medium. *Journal of Applied Mechanics*, *40*(4), 879-885.

Rana, P., & Khurana, M. (2023). Linear and weakly nonlinear investigation in thermal stability analyses of MHD convection utilizing non-Newtonian nanofluid in rotating frame of reference. *Waves in Random and Complex Media*, 1-27.

Rudraiah, N. (1984). Linear and non-linear magnetoconvection in a porous medium. In *Proceedings of the Indian Academy of Sciences-Mathematical Sciences* (Vol. 93, No. 2, pp. 117-135). Springer. New Delhi, India.

Rudraiah, N., & Vortmeyer, D. (1978). Stability of finite-amplitude and overstable convection of a conducting fluid through fixed porous bed. *Waerme und Stoffuebertragung*, *11*(4), 241-254.

Shivakumara, I.S., Mamatha, A.L., & Ravisha, M. (2016). Linear and weakly nonlinear magnetoconvection in a porous medium with a thermal nonequilibrium model. *Afrika Matematika*, *27*(7), 1111-1137.

Shubov, M.A., & Edwards, M.M. (2021). Stability of fluid flow through a channel with flexible walls. *International Journal of Mathematics and Mathematical Sciences*, *2021*(1), 8825677.

Siddheshwar, P.G., & Pranesh, S. (2004). An analytical study of linear and non-linear convection in Boussinesq–Stokes suspensions. *International Journal of Non-Linear Mechanics*, *39*(1), 165-172.

Siddheshwar, P.G., & Siddabasappa, C. (2017). Linear and weakly nonlinear stability analyses of two-dimensional, steady Brinkman–Bénard convection using local thermal non-equilibrium model. *Transport in Porous Media*, *120*, 605-631.

Srivastava, A.K., Bhadauria, B.S., & Gupta, V.K. (2012). Magneto-convection in an anisotropic porous layer with Soret effect. *International Journal of Non-Linear Mechanics*, *47*(5), 426-438.

Umavathi, J.C., & Bég, O.A. (2020). Modeling the onset of thermosolutal convective instability in a non-Newtonian nanofluid-saturated porous medium layer. *Chinese Journal of Physics*, *68*, 147-167.

Zhao, M., Zhang, Q., & Wang, S. (2014). Linear and nonlinear stability analysis of double diffusive convection in a Maxwell fluid saturated porous layer with internal heat source. *Journal of Applied Mathematics*, *2014*(1), 489279.